U-RISC: an ultra-high-resolution EM dataset challenging existing deep learning algorithms

Ruohua Shi[1†], **Wenyao Wang**[1†], **Zhixuan Li**[1], **Liuyuan He**[1], **Kaiwen Sheng**[2], **Lei Ma**[1,2], **Kai Du**[1,2], **Tingting Jiang**[1], **Tiejun Huang**[1,2]

[1]Peking University; [2]Beijing Academy of Artificial Intelligence Institution

***For correspondence:**
shiruohua@pku.edu.cn (FMS);
wangwenyao@pku.edu.cn (FS)

[†]These authors contributed equally to this work

Present address: [§]Natonal Engineering Laboratory for Video Technology, Peking University, China; [¶]Beijing Academy of Artificial Intelligence Institution, China

Abstract Connectomics is a developing field aiming at reconstructing the connection of the neural system at nanometer scale. Computer vision technology, especially deep learning methods used in image processing, has promoted connectomic data analysis to a new era. However, the performance of the state-of-the-art methods still falls behind the demand of scientific research. Inspired by the success of ImageNet, we present the U-RISC, an annotated Ultra-high Resolution Image Segmentation dataset for Cell membrane, which is the largest cell membrane annotated Electron Microscopy (EM) dataset with a resolution of 2.18nm/pixel. Multiple iterative annotations ensured the quality of the dataset. Through an open competition, we reveal that the performance of current deep learning methods still has a considerable gap with human-level, different from ISBI 2012, on which the performance of deep learning is close to human. To explore the causes of this discrepancy, we analyze the neural networks with a visualization method, attribution analysis. We find that in U-RISC, it requires a larger area around a pixel to predict whether the pixel belongs to the cell membrane or not. Finally, we integrate currently available methods to provide a new benchmark (0.67, 10% higher than the leader of competition, 0.61) for cell membrane segmentation on U-RISC and propose some suggestions in developing deep learning algorithms.

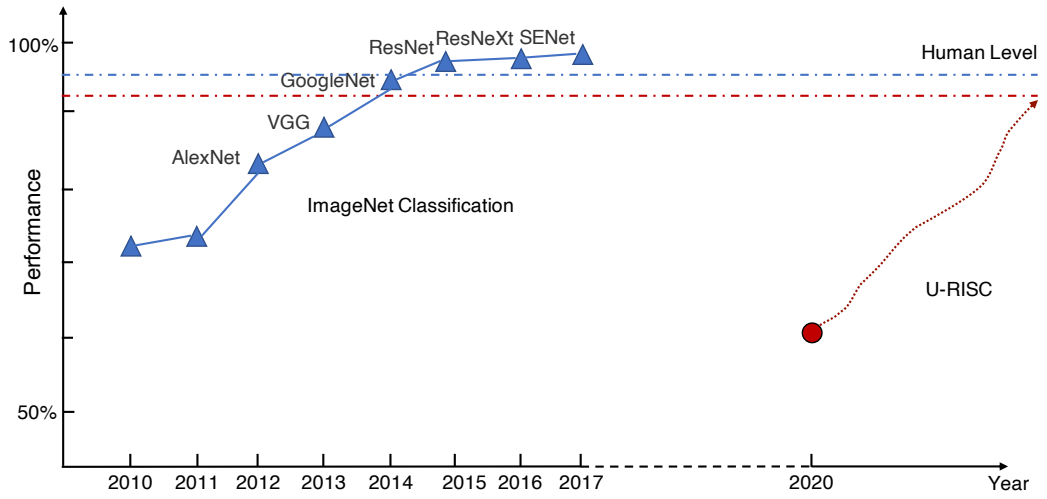

Figure 1. The history of ImageNet.

Introduction

Accurate descriptions of neurons and their connections are fundamental to modern neuroscience. By depicting neurons with the help of Golgi-staining method (***Golgi, 1885***)), Cajal could propose the classic "Neuron Doctrine" more than a century ago (***y Cajal, 1888***), which opened a new era for modern neuroscience. Nowadays, the development of electron microscopy (EM) has enabled us to further explore the structural details of the neural system at nanometer (nm) scales (***Kornfeld and Denk, 2018***; ***Shawn, 2016***) opening up a new field called "Connectomics" that aims to reconstruct every single connection in the neural system. One milestone of connectomics is the C.elegans project (***White et al., 1986***) which maps all 302 neurons and 7,000 connections in a worm. However, connectomic data increases exponentially with a higher resolution of EM and a larger neural tissue volume. Just as it took almost 15 years to complete the connectome of C.elegans, structural reconstruction for higher-level creatures is becoming more and more daunting with the explosion of connectomic data. Among many bottlenecks, accurate annotation from large amounts of EM images is the first one that has to be solved.

resnet Manual annotation of all the connectomic data is infeasible because of the high annotation cost. To reduce the burden of manual annotation for humans, one would hope to enable a machine to annotate the connectomic data with near-human performance automatically. Hopes are higher today because of the rapid development of deep learning methods. However, even with deep learning, it still requires tremendous efforts to achieve human-level performance on this challenging task. There were a few successful experiences to learn from the computer science community to make the deep learning method fully comparable to humans in connectomics. The success of deep learning methods highly depends on the amount of training data and the quality of annotation. Take the task of image classification as an example; ImageNet (***Russakovsky et al., 2014***)has set up a research paradigm of applying deep learning methods for vision tasks. In 2009, by releasing a large-scale accurately annotated dataset, ImageNet provided a benchmark (72%) for image classification. From 2010 to 2017, a challenge called "The ImageNet Large Scale Visual Recognition Challenge (ILSVRC)" was organized every year. This challenge significantly boosts the development of deep learning algorithms. Many champions of this challenge have become the milestones of deep learning methods, such as AlexNet (***Krizhevsky et al., 2012***), VGG (***Simonyan and Zisserman, 2014a***), GoogleNet (***Szegedy et al., 2015***), ResNet (***He et al., 2016***), etc. As shown in ***Figure 1***, deep learning performance on image classification performance finally exceeded human level (95%) after eight years of development. To summarize, there is a roadmap for the success of ImageNet, which includes three key steps: the first step is to establish a large-scale dataset with high-quality annotation, which is very important for deep learning. Based on the dataset, the second step is organizing a challenge that can evaluate algorithms at a large scale and allow researchers to estimate the progress of their algorithms, taking advantage of the expensive annotation effort. The third step is the design of new algorithms based on the previous two steps. Each of the three stages is indispensable.

Following the success of ImageNet, significant progress of EM automatic segmentation was achieved by the 2012 IEEE International Symposium on Biomedical Imaging (ISBI 2012), which was the first challenge on EM automatic segmentation with releasing a publicly available dataset (***Arganda-Carreras et al., 2015***) The state-of-the-art (SOTA) method exhibited unprecedented accuracy in EM cellular segmentation on the dataset of ISBI 2012. The deep learning method "U-Net" (***Ronneberger et al., 2015***), which was first proposed during the challenge, becomes the backbone of many SOTA methods in the field. However, today many deep learning methods have become "exceedingly accurate" and likely saturated at the ISBI 2012 (***Arganda-Carreras et al., 2015***). In addition, ISBI 2012 images are 512×512 pixels with a resolution of 4 nm/pixel $\times$ 4 nm/pixel, while there are many EM images with higher resolution in connectomics because enough high resolution is essential to unravel the neural structures unambiguously. For instance, 2nm has been suggested as the historical "gold standard" to identify synapses (***Debello et al., 2014***), in particular to identify gap

junctions (***Leitch, 1992***) which are common in neural tissues (***Anderson et al., 2009***). It is not clear if previous classic deep learning methods developed on EM images with relatively lower resolution can still work well on datasets with higher resolutions.

Here, to promote the deep learning algorithms in EM datasets, we initiate a new roadmap: We first annotated the retinal connectomic data, RC1, from rabbit (***Anderson et al., 2011***) and presented a brand new annotated EM dataset named U-RISC (Ultra-high Resolution Image Segmentation dataset for Cell membrane). Compared with ISBI 2012, U-RISC has a higher resolution of 2.18 nm/pixel and a larger size of 9958 $\times$ 9959 pixels. The precision of annotation was ensured by multi-steps of iterative verification, costing over 10,000 hours in total. Next, based on U-RISC, a competition of cellular membrane prediction was also organized. Surprisingly, from 448 domestic participants/teams, the top performance of deep learning methods on U-RISC ($\sim$ 0.6, F1-score) was far below the human-level accuracy (> 0.9), in contrast with the near-human performance of deep learning methods in ISBI 2012. We then made fair comparisons between ISBI 2012 and U-RISC with the same segmentation methods, including U-Net. The comparison results confirmed that U-RISC indeed provides new challenges to existing deep learning methods. U-Net, for example, drops from 0.97 in ISBI 2012 to 0.57 in U-RISC. To further explore how these methods work on segmentation tasks, we introduced a gradient-based attribution method, integrated gradient (***Sundararajan et al., 2017***), to analyze ISBI 2012 and U-RISC. The result showed that when deciding on whether a pixel belonged to the cell membrane or not, deep learning methods represented by U-Net would refer to a larger attribution region on U-RISC (about four times on average) than that on ISBI 2012. It suggests that the deep learning methods might require more background information to decide the segmentation of the U-RISC dataset. Finally, we integrated current available advanced methods, combining U-Net and transfer learning recently introduced (***Conrad and Narayan, 2021***), and provided a benchmark (0.6659), about 10% higher than the leader board (0.607), for U-RISC.

Overall, our contribution in this work lies mainly in the following three parts: (1) we provided the community a brand new public available annotated mammalian EM dataset with known highest resolution ($\sim$ 2.18 nm/pixel) and largest image size (9958 pixel $\times$ 9959 pixel); (2) we organized a competition and made a comprehensive analysis to reveal the challenges of U-RISC for deep learning methods; (3) we improved the benchmark with 10% to the F1-score of 0.6659. In discussion, we proposed further suggestions for improving segmentation methods from perspectives of model design, loss function design, data process, etc. We hope our dataset and analysis can help researchers gain insights into designing more robust methods, which can finally accelerate the speed of untangling brain connectivity.

Results

The largest ultra-high resolution EM cell membrane segmentation dataset

Along with this paper, we proposed a new EM dataset with cell membrane annotated: Ultra-high Resolution Images Segmentation dataset for Cell membrane (**U-RISC**). To our best knowledge, U-RISC has the highest resolution among the public available annotated EM datasets (see ***Figure 2***(A) as an example). It is annotated upon the rabbit retinal connectomic dataset RC1 (***Anderson et al., 2011***) with a 2.18 nm/pixel resolution at both x and y axes. The size of individual image and the total number of images in U-RISC both exceed the published dataset by far, taking ISBI 2012 as an example (***Figure 2***(C)) (120 pairs of 9958 (px) $\times$ 9959 (px) images in U-RISC and 30 pairs of 512 (px) $\times$ 512 (px) images in ISBI 2012). One characteristic of U-RISC is that cell membranes only cover a small area of the images, making it an imbalanced dataset for deep learning (an average of 5.10% $\pm$ 0.02 in U-RISC compared with 21.65%$\pm$ 0.02 in ISBI 2012).

We employed an iterative manual annotation procedure to ensure the quality of annotation. Because of the difficulty of distinguishing cell membrane from organelle membrane, special attention was paid to exclude organelle membrane from annotation (***Figure 3***(A)). In practical connectomic research, the image quality can be affected by many reasons like insufficient staining, thick section,

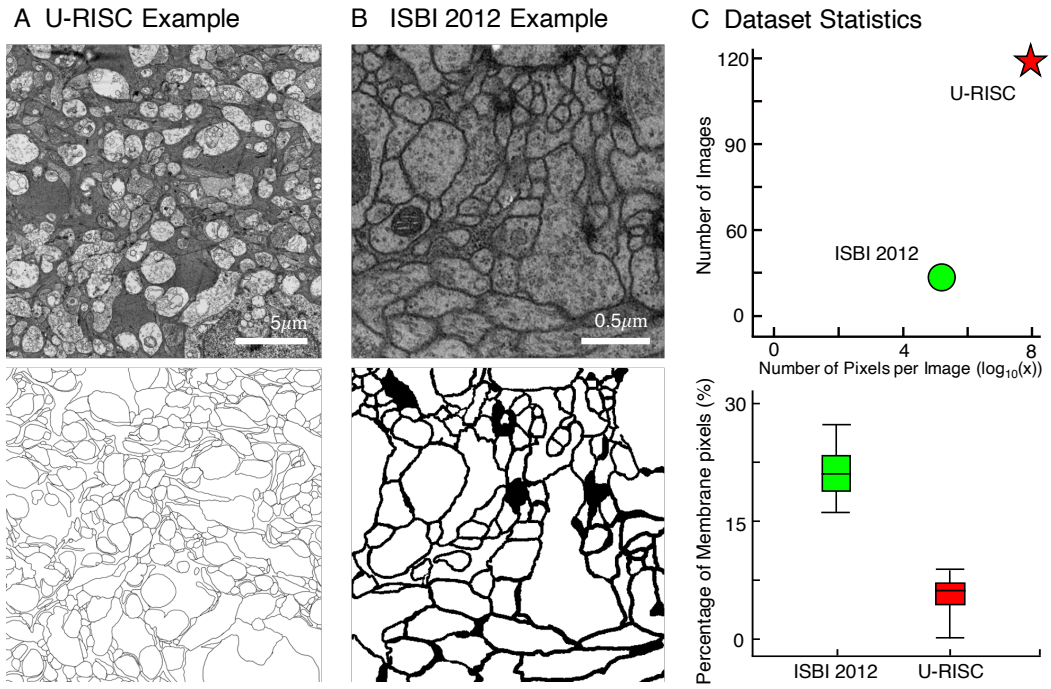

Figure 2. Comparison between U-RISC and ISBI 2012. (A and B) An example of U-RISC and ISBI 2012 data includes the raw EM image (top) and the corresponding annotation result (bottom). Black pixels in annotation results represent cellular membranes. (C) (Top) Both the number and size of images in U-RISC surpass those in ISBI 2012. (Bottom) The proportion of annotated pixels, 5.10%±0.02 in ISBI 2012 and 21.65%±0.02 in U-RISC, making latter a more imbalanced dataset.

etc. Considering this, we retained several images with low quality in U-RISC to make the dataset closer to the actual situation. Annotation on these images costs more time and caution (***Figure 3***(B)). Labeling errors could be detected and then corrected in each round of iteration (***Figure 4***). For scientific research reasons, the human labeling process is very valuable for uncovering the human learning process. Therefore, the intermediate annotated results were also reserved for public release at https://brain.baai.ac.cn/biodb-rabbit-details.html.

Ultra-high resolution EM images segmentation benchmark

To investigate the performance of the deep learning methods on U-RISC and propose a benchmark, a competition about cellular membrane segmentation was organized [1] by BAAI (Beijing Academy of Artificial Intelligence Institution, Beijing, China) and PKU (Peking University, Beijing, China). In total, 448 participants took part in the competition, mainly from domestic competitive universities, research organizations, and top IT institutions.

There were two tracks in the competition (***Table 1***): Track 1 used original images with the size of 9958 (px) × 9959 (px) as training and testing datasets. In Track 2, images were downsampled to the size of 1024 (px) × 1024 (px). The purpose of Track 2 was to allow researchers with limited computational resources to participate in the competition. A final round of human annotation was used as ground truth to evaluate the algorithms, and an F1-score was applied as the evaluation metric (for details, please see Methods and Materials).

Surprisingly, from the competition, top 6 teams in each track gained an F1-score around 0.6 on U-RISC, which was far below the human levels (0.92 and 0.99 during the first and second rounds of annotation, respectively). However, previous research has shown that the performance of the top teams in ISBI 2012 have already been reasonably close to the human level (***Arganda-Carreras et al.,***

[1] https://www.biendata.xyz/competition/urisc/

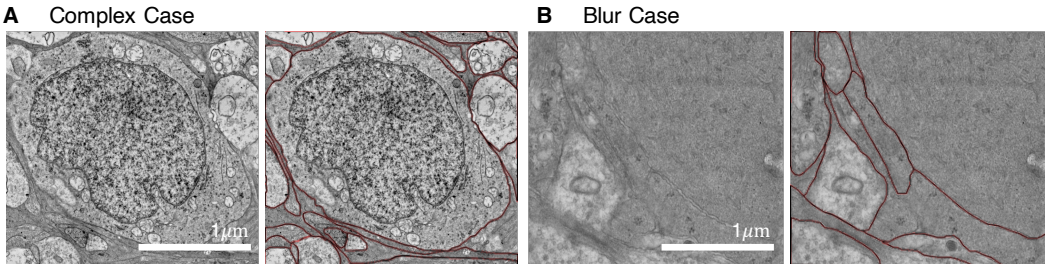

Figure 3. Examples of images with their annotations. (A) Organelle membranes were cautiously avoided to be annotated. (B) More time and patience were needed to annotate the image with low contrast.

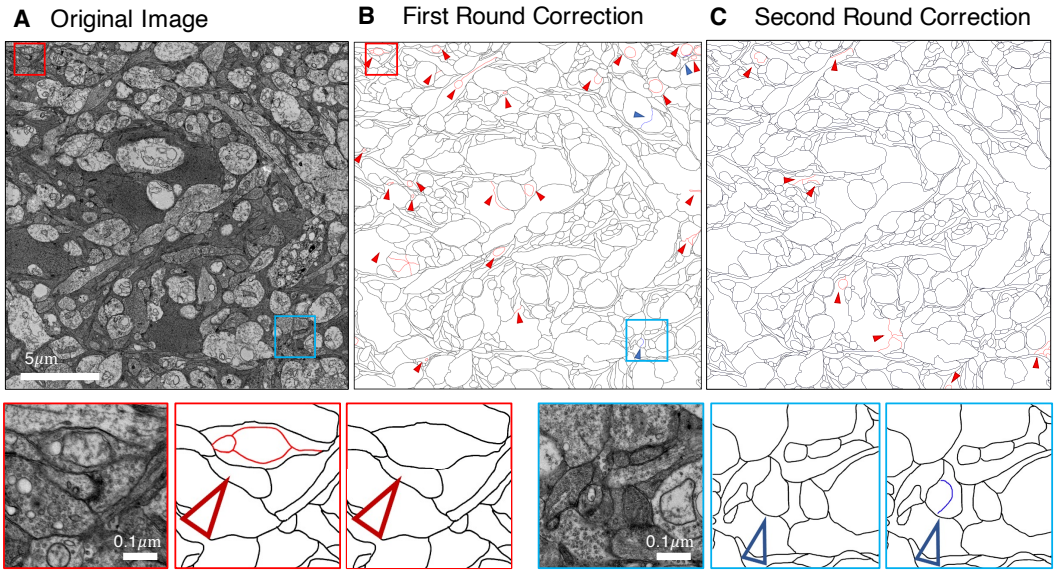

Figure 4. Example of iterative human annotation. (A) Original image to be annotated. (B) Many errors were found out in the first round of annotation. (C) After correction, much fewer errors were detected in the second round of annotation, and the correction results were served as the final annotation. Red small triangles and boxes indicate false positive errors (enlargement in the bottom left), blue for false-negative errors (enlargement in the bottom right).

2015). We surveyed the top 6 teams to investigate the performance gap between the methods and humans on U-RISC. It indicated that a variety of current popular approaches to segmentation had been utilized(***Figure 5***). From the choice of models (***Figure 5***(A)), the participant had used current popular image segmentation networks, such as U-Net (***Ronneberger et al., 2015***), Efficientnet (***Tan and Le, 2019***) and CASENet (***Zhiding Yu et al., 2017***). For backbone selection, ResNet (***He et al., 2016***) and their variants were the most chosen architectures for backbone selection. Data augmentation was ubiquitously applied to improve the generalization of the models from the selection of data processing techniques. About 13% of the participants used Hypercolumns (***Hariharan et al., 2015***) to improve the expressiveness of the model. From the design of loss function, functions that can adjust penalty ratios according to sample distributions were applied to reduce the effect of sample imbalance, such as Dice loss (***Dice, 1945***), Focal loss (***Lin et al., 2017***), and BCE loss (***Cui et al., 2019***).

Table 1. Leaderboard of Track 1 and Track 2.

Track 1 (Original)			Track 2 (Downsample)		
Team Name	Institution	F1-score	Team Name	Institution	F1-score
Human 1st		0.92128± 0.012	Human 1st		0.96915± 0.014
Human 2nd		0.99334± 0.008	Human 2nd		0.99891± 0.003
SCP173	Tencent[1]	0.60704± 0.043	horch	UCAS[2]	0.56932± 0.053
yangsenwxy	SCU[3]	0.60701± 0.042	deadline	NJU[4]	0.56213± 0.055
SpongeBobbb	HDU[5]	0.60480± 0.042	SpongeBobbb	HDU[5]	0.56136± 0.049
VIDAR	USTC[6]	0.60303± 0.041	VIDAR	USTC[6]	0.55170± 0.046
deadline	NJU[4]	0.60066± 0.045	archer	THU[7]	0.55107± 0.047
Chasingstar	JLU[8]	0.59647± 0.044	scu_ws	SCU[3]	0.54847± 0.053

Mean and standard error are computed over test images.

And Adam (***Kingma and Ba, 2014***) was shown to be the most chosen optimization method.

The analysis suggested that even though participants considered many popular methods, their performance was still not satisfactory and varied only slightly between each other. To identify whether this is because of the challenges of U-RISC or the methods themselves, we picked out three widely used methods: U-Net (***Ronneberger et al., 2015***), LinkNet (***Chaurasia and Culurciello, 2017***), and CASENet (***Zhiding Yu et al., 2017***). We conducted a fair comparison between the performance of each method on U-RISC (Track 1) and ISBI 2012. Results showed that these methods could reach over 0.97 (F1-score) in ISBI 2012, but only around 0.57-0.61 in U-RISC (***Table 2***), which confirmed that the performance gap in competition comes from the challenges of U-RISC.

Table 2. F1-scores in U-RISC and ISBI 2012.

Method	U-RISC	ISBI 2012
LinkNet-*	0.60701± 0.063	0.97246± 0.08
CASENet-*	0.60065± 0.053	0.97132± 0.08
U-Net-*	0.57123± 0.049	0.97010± 0.09

What are the unique challenges brought by U-RISC to deep learning algorithms? Two types of errors were analyzed first: false-positive errors, which led to incorrect membrane predictions, and false-negative errors, which caused continuity of cell membrane. According to our analysis, both false-positive errors (pink boxes) and false-negative errors (orange boxes) were common in U-RISC, which were rare in ISBI 2012 (***Figure 6***(B) (C)). Further investigations for the networks are required to explore the reason and find ways to reduce the errors.

Attribution analysis of deep learning method on U-RISC and ISBI 2012

To acquire a deeper understanding of the different performances in U-RISC and ISBI 2012, we performed an attribution analysis (***Ancona et al., 2019***) on the trained U-Net. We selected the gradient-based attribution method, **integral gradient (IG) (*Sundararajan et al., 2017*)**, which is widely applied on explainable artificial intelligence, such as understanding feature importance (***Adadi and Berrada, 2018***), identifying data skew (***Clark et al., 2019***), and debugging model performance (***Guidotti et al., 2018***). In brief, IG aims to explain the relationship between predictions and input features

[1]Tencent Holdings Ltd (China)
[2]University of Chinese Academy of Sciences (China)
[3]Sichuan University (China)
[4]Nanjing University (China)
[5]Hangzhou Dianzi University (China)
[6]University of Science and Technology of China
[7]Tsinghua University (China)
[8]Jilin University (China)

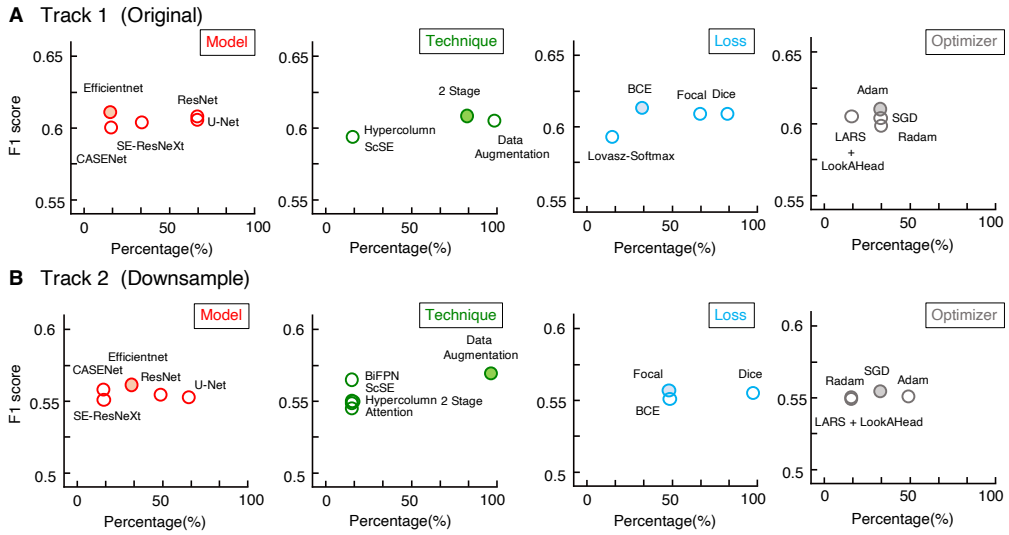

Figure 5. Mean F1 scores of teams with different methods used. (A and B) The statistics of Track 1 and Track 2, respectively. The X-axis represents the proportion of the team with the method, Y-axis represents the average of F1 scores.

based on gradients(*Figure 7*(A)). The IG output is plotted in **Attribution Field** A to reflect their contribution to the final prediction. In the heatmap, each pixel was assigned with a normalized value between [-1,1]. With IG, we analyzed the attribution field of each predicted pixel of U-Net in U-RISC and ISBI 2012. Color and shade were used to represent the normalized contribution values in attribution fields *Figure 7*(B). For a fair comparison between U-RISC and ISBI 2012, areas of **Pixel Attribution Field** S_k's areas were converted to physical size according to their respective resolutions.

Figure 8 shows the examples of attribution fields, where bounding boxes with different colors represented different pixel classifications, green for a correct predicted pixel, orange for a false positive error, and pink for a false negative error. We noticed that the areas of attribution fields S_k of two datasets were both relatively minor to the whole images (*Figure 7*(B)). For example, at the threshold of $k > 0.01$, the S_k of the correct cases (the green bounding box in *Figure 8* in U-RISC and ISBI 2012 accounted for only 5.1% and 0.8% relative to the whole image). This suggested that U-Net would focus on local characteristics within small areas of the images when making predictions. In addition, we found that U-Net would refer to larger area when making decisions on U-RISC compared with ISBI 2012. The averaged S_k of each predicted pixel in U-RISC was significantly larger than that in ISBI 2012, specifically 46000 nm^2 in U-RISC and 10300 nm^2 in ISBI 2012. Taken together, U-Net would predict, according to local information around the pixel, the average attribution filed was larger in U-RISC than that of ISBI 2012, which indicates that more information is required for the segmentation in U-RISC.

U-Net-transfer model achieve the state-of-the-art result on U-RISC benchmark

Considering both the comprehensive analyses of competition and attribution analysis, we integrated outperformed methods to develop our method (*Figure 9*(A)). For basic segmentation architecture, we chose U-Net due to its better characteristic extraction ability. Many valuable techniques were also considered, including cross-crop strategy for saving computational resources and data augmentation to increase data diversity. We chose both focal loss and dice loss to deal with the imbalance of samples for loss function design. Some parameters used for training were also optimized, such as batch-size/GPU (4) and the number of GPUs (8). For more details, please refer to the part of Segmentation Networks in Methods and Materials. Especially, recent research has shown that

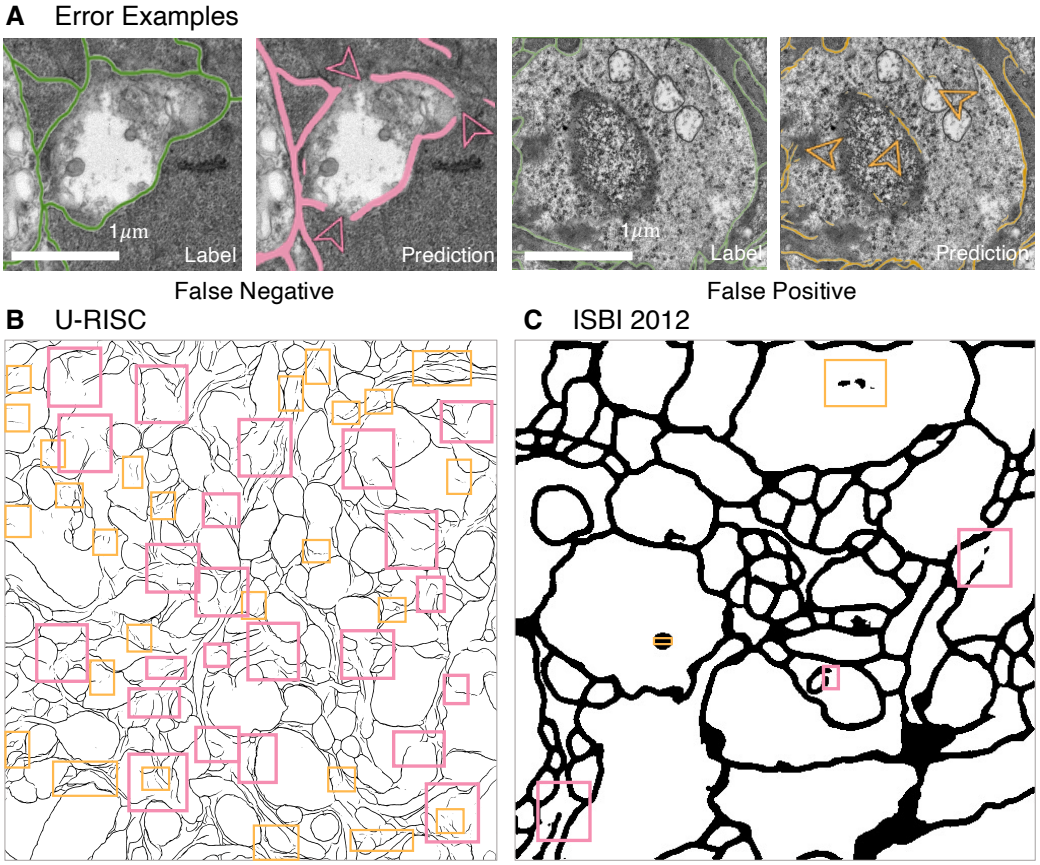

Figure 6. Errors in segmentation predictions of U-RISC and ISBI 2012. (A) The examples of False Positive and False Negative errors. (B and C) The examples of two errors in the segmentations of U-RISC and ISBI 2012. Pink arrows and lines represent false-negative errors, and orange represents false positive errors.

Figure 6–Figure supplement 1. Supplements for segmentation predictions of U-RISC.

Figure 6–Figure supplement 2. Supplements for segmentation predictions of ISBI 2012.

transfer learning with domain-specific annotated datasets could be effective in elevating deep learning models' performance (***Conrad and Narayan, 2021***). Therefore, we introduced a pre-trained model, trained with MoCoV2 (***He et al., 2020b***) on CEM500K (***Conrad and Narayan, 2021***). The segmentation result showed that the F1 scores of our method were 10% higher than the leader of competition (0.66 vs 0.61 in ***Table 2***). Thus we provide a new benchmark on the cellular membrane segmentation of U-RISC.

Discussion

This paper first proposed the U-RISC, a cell membrane EM dataset created through intensive and elaborate annotation. The dataset is characterized by the highest resolution and the largest single image size compared with other current public available annotated EM datasets. Next, we organized a segmentation competition on U-RISC and proposed the benchmark. During the competition, we noticed that the performances of popular deep learning methods were far below that of humans, which motivated us to explore the causes. Thus, we carried out a comprehensive survey on the deep learning methods participants applied in the competition. To our surprise, methods such as U-Net, LinkNet, and CASENet exhibited a significant drop of F1-score on U-RISC compared with ISBI 2012, from 0.9 to 0.6. To explore the mechanisms underlying this discrepant performance, we introduced a gradient-based attribution method, integrated gradient. Through attribution analysis of U-Net,

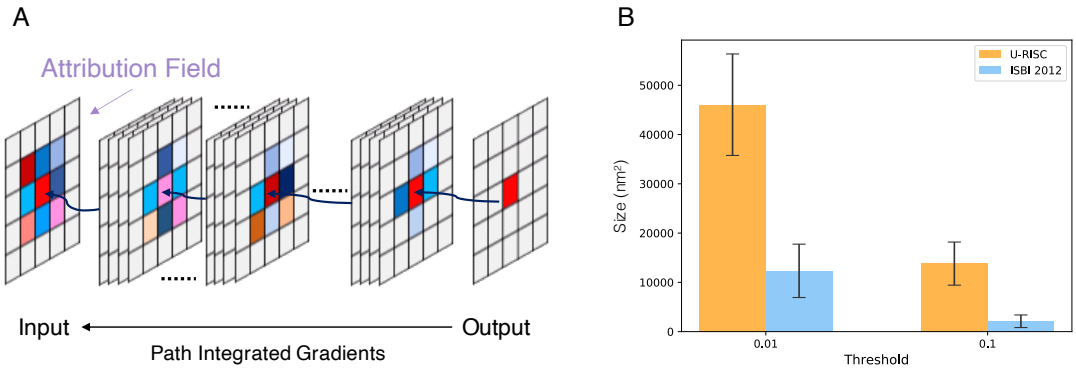

Figure 7. Attribution analysis. (A) Integrated gradients attribution method. (B) Statistics of attribution filed for U-RISC and ISBI 2012.

we found the average pixel attribution field of U-RISC is larger than that of ISBI, corresponding to the size of cellular structure, and both of them are relatively small to the whole image size. By integrating currently available methods, we improve the benchmark to 0.67, about 10% higher than the top leader from the competition. Based on the analysis in this paper, here we raise some considerations about the challenges for deep learning-based segmentation algorithms brought by U-RISC and propose several suggestions for improving EM segmentation methods.

Challenges for Deep Learning-based Segmentation

Benchmark showed that the segmentation performance of deep learning algorithms on U-RISC was still far behind the human level. U-RISC poses challenges for deep learning-based segmentation in the following aspects: (1) high computational costs needed to deal with images of large size, (2) the extreme sample imbalance caused by low ratio of cellular membrane pixels in the whole image, (3) side effects of typical data processing methods.

Deep learning itself is already a computationally intensive method. It would require more computational resources to process the images with the much larger size in U-RISC. In practical terms, taking U-Net as an example, processing a 1024 (px) ×1024 (px) image requires a GPU with 12GB memory. This memory is enough to deal with the images in ISBI 2012, of which the size is 512 (px) ×512 (px). But the size of a single image in U-RISC is 9958 (px) ×9959 (px), which is far beyond the processing ability of the commonly used 12 GB memory GPU. Therefore, the additional computational burden brought by U-RISC raises the first challenge for deep learning-based segmentation.

The problem of imbalanced samples widely exists in computational vision tasks (***Alejo et al., 2016***; ***Li et al., 2010***; ***Zhang et al., 2020***), which should be considered when designing algorithms. Cellular membrane segmentation is a typical situation of sample imbalance because cellular membrane only occupies a small proportion of the whole cell structure. According to statistics, the pixels belong to the cellular membrane account for 21.65% of the entire pixels of ISBI 2012.But the proportion in U-RISC is much smaller, 5.10%, making U-RISC an extremely imbalanced dataset. Pre-existing solutions were mainly proposed from several aspects: loss function design (***Lin et al., 2017***; ***Cui et al., 2019***), data augmentation (***Yoo et al., 2020***), under/over-sampling (***Fernández et al., 2018***; ***Yen and Lee, 2009***), and semantically multi-modal approaches (***Zhu et al., 2020***). Even though the participants in the competition already used these approaches, the final results showed limited improvement of segmentation. So the imbalanced problem of U-RISC is yet to be solved and becomes another challenge for deep learning-based segmentation.

Proper data processing is essential and helpful to deep learning algorithms. For example, a downsampling process on the raw images with an enormous size is commonly adopted in

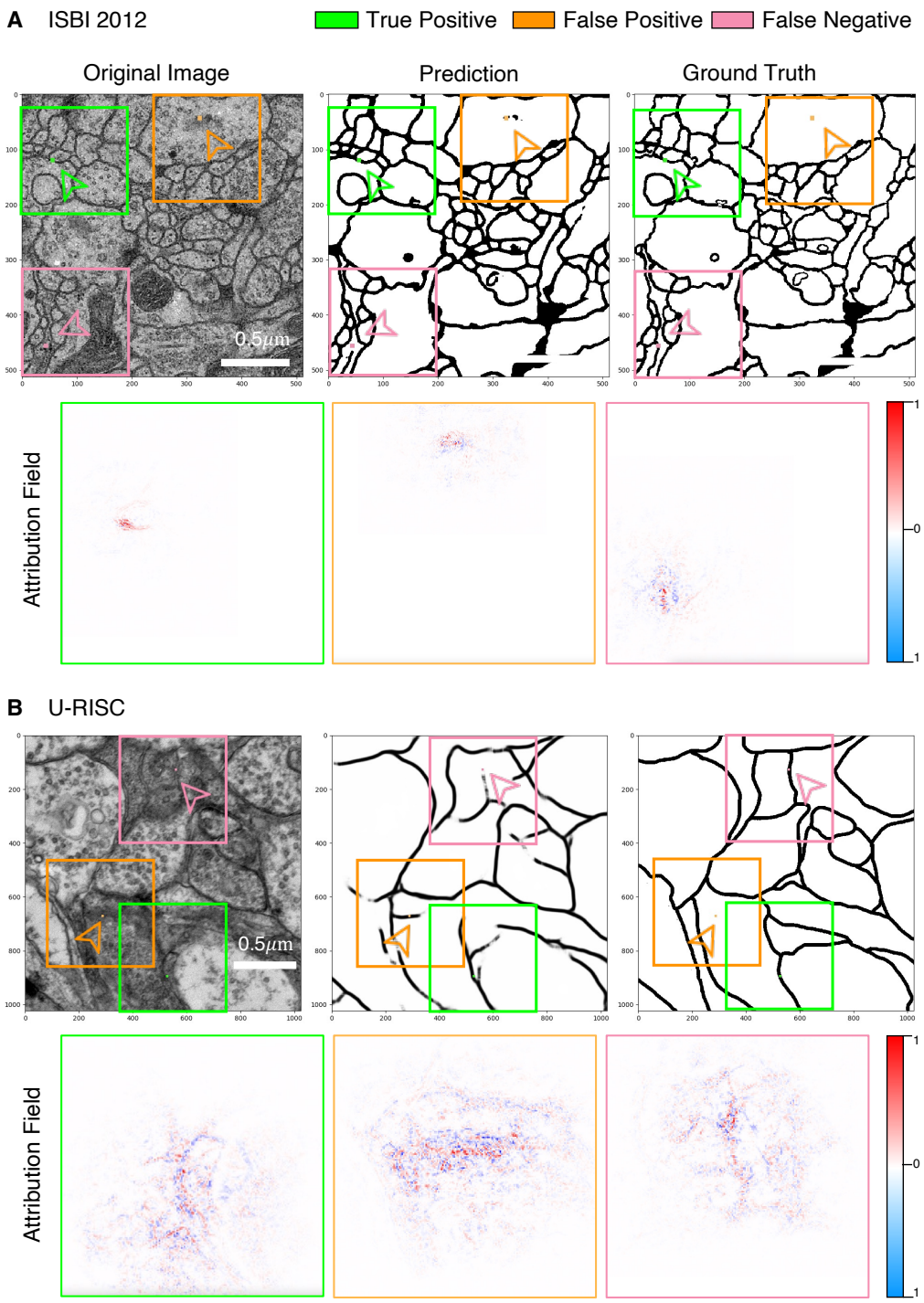

Figure 8. Attribution analysis. (A and B) Attribution fields of ISBI 2012 and U-RISC dataset. The first line represents the original image, network prediction result and annotation respectively. The pixels pointed by green (correct cell membrane pixel), orange (false positive predicted pixel) and pink (false negative predicted pixel) arrows are the prediction points used in attribution method. Images in the three color boxes with the same size in the second line represent the attribution field corresponding to the above three pixels. Blue means the network is likely to predict the pixels as cell membrane, while opposite for red.

Figure 8–Figure supplement 1. Supplements for attribution analysis on ISBI 2012.

Figure 8–Figure supplement 2. Supplements for attribution analysis on U-RISC.

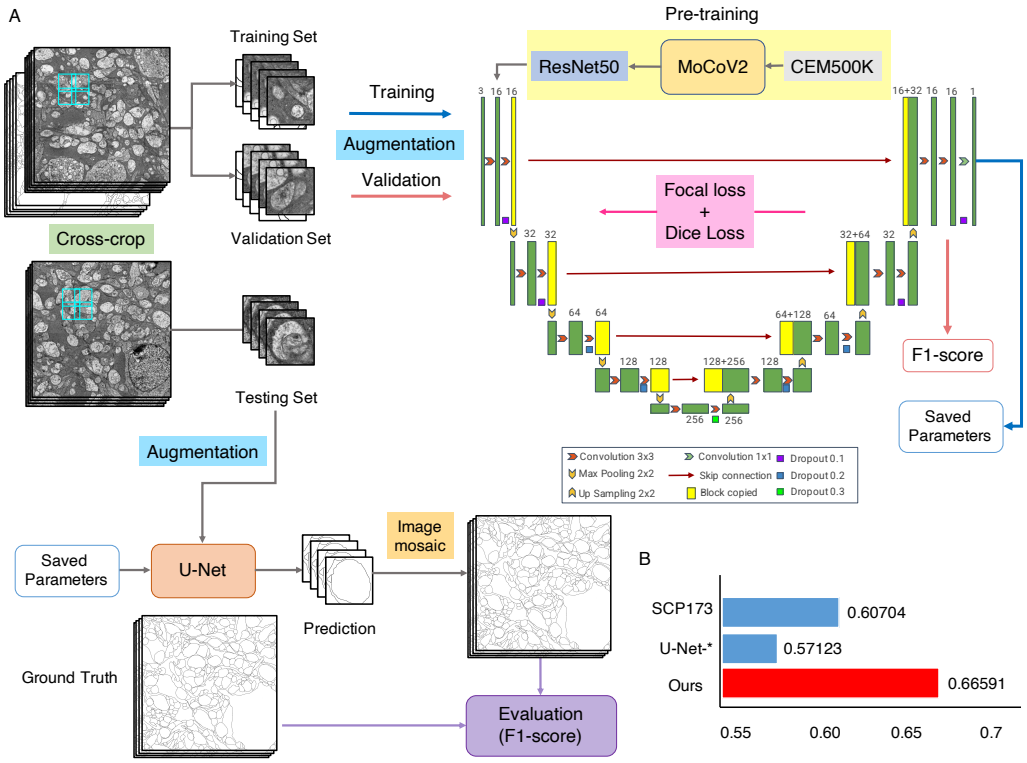

Figure 9. The U-Net-transfer method achieves the best performance on U-RISC. (A) The pretraining, training, and testing processing for U-Net. (B) The comparison of the F1-scores. "SCP-173" represents the top performance in the competition. U-Net-* represents the performance in ***Table 2***.Ours represents the performance of the U-Net-transfer method in this section.

segmentation tasks (***Marin et al., 2019***; ***Chen et al., 2014***). And in Track 2 of the competition, we used the downsampled dataset to reduce computational consumption as usual. Surprisingly, we found that the F1-score of the same method dropped as well as the overall performance decreased in Track 2 compared with Track 1. We speculated a key reason might be the degradation of image quality from track 1 to Track 2. We confirmed the quality reduction through 4 representative indexes, including Brenner (***Subbarao and Tyan, 1998***), Variance (***Subbarao and Tyan, 1998***), SMD2 (***Thakkinstian et al., 2005***), and Vollath (***Vollath, 2008***) (shown in Appendix). More caution should be paid when using traditional data processing methods, and more advanced data processing theories are expected from this point of view.

Suggestions for the Improvement of Segmentation Methods

To some degree, increasing computational resources is a possible way to cope with the challenges mentioned above. However, it might not be easy for all the community researchers to access sufficient computational power; therefore innovations in algorithms are still crucial for our future success. To improve the performance of deep learning in EM segmentation, we provide several suggestions for developing deep learning algorithms from the following perspectives: model design, training techniques, data processing, loss function design, and visualization tools.

Model Design. As shown in the attribution analysis, the current models for segmentation, such as U-Net (***Ronneberger et al., 2015***), Efficientnet (***Tan and Le, 2019***) , and CASENet (***Zhiding Yu et al., 2017***), are designed to focus on local information to make a prediction. However, in a high-resolution image, other structures, like organelle membrane and synaptic vesicles, might share similar features with the cellular membrane in a local scale, which leads to false-negative results. And this constitutes one of the major error types in the competition. Therefore, it might not be enough for the classifiers of a model to make correct decisions with only local features. And studies have shown that models using global information could improve performance greatly (***Liu et al., 2018b***, ***2020***; ***Wang et al., 2019***). Therefore, more global information could also be considered in the future design of the segmentation network.

Training Techniques. Skillful training techniques also can be helpful to improve the segmentation performance. According to our survey, a two-stage training strategy could be much better than a single-stage training strategy. Recent work also suggests that pretraining with domain-specific datasets can help network learning domain features (***Conrad and Narayan, 2021***). Besides that, much experience can be learnt from existing training methods. The Hypercolumns module (***Hariharan et al., 2015***) was used to accelerate the convergence of training by combining features at different scales, and the combination of features from different scales can help bring in global information. ScSE (***Roy et al., 2018***) module introduces attention mechanism into network, thus bringing in global information. Hybrid architectures can also be considered because of its ability to expand the receptive field (***Goceri, 2019***). In a word, improvement can be made at the phase of training by utilizing advanced training techniques.

Data Processing. Data processing is commonly used in deep learning, while traditional downsampling methods were shown to have side effects in the competition. To alleviate the side effects, some quality enhancing methods for downsampled images could be expected, such as edge and region-based image interpolation algorithms (***Asuni and Giachetti, 2008***; ***Hwang and Lee, 2004***), low bit rate-based approaches (***Wu et al., 2009***; ***Lin and Li Dong, 2006***), and quality assessment researches (***Vu et al., 2018***; ***Wang and Bovik, 2006***; ***Wang et al., 2003***). Meanwhile, other data processing methods can also be taken into account. Take data augmentation as an example; by augmenting the training data randomly, the dependence of the model on specific attributes can be reduced, which can be beneficial in EM segmentation with many imbalanced samples.

Loss Function Design. Loss function design is another important part of deep learning. But many current loss functions have their own disadvantages in our competition. For example, Dice loss (***Dice, 1945***) was designed to optimize F1-score directly, without consideration of data imbalance. Focal loss (***Lin et al., 2017***) and BCE loss (***Cui et al., 2019***) was used in the competition

to care more about data imbalance by giving different penalty according to sample difficulty, but the improvement is limited as the results have shown. A better design of loss function should take overall consideration of both sample imbalance and evaluation criteria. While the most common evaluation criterion, F1-score, a pixel-based statistic, is inconsistent with subjective human feeling to some extent. It might be a major cause of the performance gap between humans and algorithms. Some other structure-based criteria have appeared, such as V-Rand and V-info (***Arganda-Carreras et al., 2015***) integrating skeleton information of cell membrane, and ASSD (***Zhang, 1996***) considering the distance of point sets.

Visualization tools. Visualization tools can help us have a better understanding of the network. In this paper, with IG, we could learn the attribution fields of U-Net from the view of gradient, which inspires us to improve deep learning methods by paying more attention to global information. In comparison, many other visualization tools are starting from other characteristics of the network. Layer-wise relevance propagation (LRP) (***Bach et al., 2015***) and deep Taylor decomposition (DTD) (***Montavon et al., 2017***) get attribution distribution by modifying propagation rules. Information-based method IBA (***Schulz et al., 2020***) restricts the flow of information to accomplish attribution fields. Combining different visualization tools can help to promote much more insightful inspiration in improving deep learning methods.

Overall, we provide an annotated EM cellular membrane dataset, U-RISC. It indeed brings many challenges for deep learning and promotes the development of deep learning methods for segmentation.

Methods and Materials

Dataset

The U-RISC dataset was annotated upon RC1, a large-scale retinal serial section transmission electron microscopic (ssTEM) dataset, publicly available upon request and detailedly described in the work of ***Anderson et al.*** (***2011***). RC1 came from the retina of a light-adapted female Dutch Belted rabbit after in vivo excitation mapping. The imaged volume represents the retinal tissue with a diameter of 0.25 mm, spanning the inner nuclear, inner plexiform, and ganglion cell layers. Serial EM sections were cut at 70-90 nm with a Leica UC6 ultramicrotome and captured at the resolution of 2.18 nm/pixel across both axes using SerialEM (***Mastronarde, 2005***). In RC1, there are in total 341 EM mosaics generated by the NCR Toolset (***Anderson et al., 2009***), and we clipped out 120 images in the size of 9958 (px) $\times$ 9959 (px) from randomly chosen sections.

To annotate cell membrane with high quality on 120 images, we launched an iterative annotation project that lasted for three months. All the annotators were trained to recognize and annotate cellular membrane in EM images, but only two-thirds of all, 53 annotators, were finally qualified to participate in the project according to their annotation results. In the iterative annotation procedure, each EM image would undergo three continuous rounds of annotation with the guidance of blind review. The final round of annotation was regarded as the "ground truth". While since the first two rounds are valuable for analyzing the human learning process, we also reserved the intermediate results for public release. All of the U-RISC datasets are released on https://www.biendata.xyz/competition/urisc/.

Competition

The goal of the competition was to predict cell membranes in the EM images of U-RISC. Participants were required to return images depicting the boundary of all neurons. F1-score was selected as the evaluation criterion for the accuracy of the results. There are two tracks in the competition, images in Track 1 were kept as the original size (9958 (px) $\times$ 9959(px)), images in Track 2 were downsampled to the size of 1024 (px) $\times$ 1024 (px). Fifty images, 30 as the training dataset and 20 as the test dataset, were released in Track 1. And Track 2 contained 70 images in total, 40 training images, and 30 testing images. The training dataset included EM images with their corresponding ground truth,

while the ground truth of the test dataset was kept private. In both tracks, ten images from the training dataset served as the validation dataset for the participants to monitor and develop their models. No statistical methods were used to determine the assignment of images in the whole arrangement.

Segmentation Networks

We conducted experiments to compare the performance of the same methods on U-RISC (Track2) and ISBI 2012. Three representative deep learning networks were considerred ***Table 2***, U-Net (***Ronneberger et al., 2015***), LinkNet (***Chaurasia and Culurciello, 2017***), and CASENet (***Zhiding Yu et al., 2017***). The three networks are all pixel-based segmentation networks. To be specific, given the input image x, the goal of the networks is to classify the corresponding semantic cell membrane pixel by pixel. For the input image x and classification function $F(x)$, $Y\{p|X,\Theta\} \in [0,1]$ is taken as the output of the network, which represents the edge probability of the semantic category of the pixel p. Θ are the parameters in the network and are optimized in the training processes. Architectures of the three networks are described as follows.

U-Net. U-Net (***Ronneberger et al., 2015***) is a classical fully convolutional network (that is, there is no fully connected operation in the network). The model is composed of two parts: contracting path and expansive path. The contracting path follows the typical architecture of a convolutional network. At each downsampling step, U-Net double the number of feature channels to gain a concatenation with the correspondingly cropped feature map from the contracting path. At the final layer a 1×1 convolution is used to map each 64-component feature vector to the desired number of classes. In total the network has 23 convolutional layers. We use ResNet50 as its encoder.

LinkNet. The model structure of LinkNet (***Chaurasia and Culurciello, 2017***) is almost similar to U-Net, which is a typical encoder-decoder structure. The encoder starts with an initial block which performs convolution on input image with a kernel of size 7×7 and a stride of 2. This block also performs spatial max-pooling in an area of 3×3 with a stride of 2. The later portion of encoder consists of residual blocks and are represented as encoder-block. To reduce parameters, LinkNet uses ResNet18 as its encoder.

CASENet. CASENet (***Zhiding Yu et al., 2017***) is an end-to-end deep semantic edge learning architecture adopting ResNet-101 as backbone. The classification module here consists of a 1×1 convolution and a bilinear interpolation up-sampling layer to generate M active images, each image size is the same as the original image. Each residual block is followed by a classification module to obtain five classification activation graphs. Then, a sliced concatenation layer is used to fuse the M classification activation graphs, and finally a $5M$ channel activation graph is obtained. The activation graphs are used as the input of the fused classification layer to obtain a M-channel activation graph. The fusion classification layer is convolution of M group 1×1.

Transfer learning. The pre-trained model from (***Conrad and Narayan, 2021***) was used in our method, specifically MoCoV2 (***He et al., 2020b***) and CEM500K (***Conrad and Narayan, 2021***) were respectively selected as the pretraining method and dataset.

Training settings. For each dataset, same training and testing data distribution were utilized on the three methods. For U-RISC, during the training, the original images were cut into 1024 × 1024 patches with overlaps, and the patches was randomly split assigned in numbers of according to the ratio of 50,000/20,000 to yield the training set and the validation set, respectively. For ISBI 2012, 20 images were used for training and 10 images were used for testing.

Loss function and optimization. For each algorithm, we use the same loss functions and optimization method. Specifically, focal loss and dice loss are chosen. Define y as the ground truth segmentation and y' is the predicted segmentation. The calculations of focal loss and dice loss are:

$$L_{\text{Focal}} = -(1-\hat{y})^{\gamma}\log(\hat{y}) \tag{1}$$

$$L_{\text{Focal}} = -(1-\hat{y})^{\gamma}\log(\hat{y}) \tag{2}$$

Table 3. Parameter settings.

Parameters	U-Net-*	CASENet-*	LinkNet-*	U-Net-transfer
Data augmentation	√	√	√	√
Pre-training	-	-	-	√
Learning Rate	1e-3	1e-7	5e-4	2e-5
Batch Size	4	2	1	4
GPUs	4	4	4	8
Epoch	100	300	300	50
Worker	16	16	8	32

And the final loss function is the summation of the two losses with the proportion of $1 : \lambda$. That is $L = L_{\text{Focal}} + \lambda L_{\text{Dice}}$. We set $\lambda = 1$ in these experiments. When optimizing the parameters in the network, we chose Adam (***Kingma and Ba, 2014***) as the optimizer.

Parameter settings. The parameters, training techniques, and loss functions were the same in both datasets. Data augmentation (random horizontal/vertical flip, random rotation, random zoom, random cropping, random cropping, random translation, random contrast, and random color jitter) were used. Four Nvidia V100 GPUs were used for training. In the testing stage, the original image was cut into the same size of training image, and the patch was tested. These patches were eventually mosaiced back to the original size for evaluation. The parameters settings are shown in ***Table 3***. Mean value and standard error are computed over testing images of each dataset. The methods with "-*" in the table represent that they are implemented by ourselves.

Image definition criteria

Four representative image definition criteria **Brenner** (***Subbarao and Tyan, 1998***), **SMD2** (***Thakkinstian et al., 2005***), **Variance** (***Saltelli et al., 2010***), and **Vollath** (***Vollath, 2008***) were used for analyzing the effects of downsampling on EM images. The former two consider the difference and variance of gray values between adjacent pixels, while the latter two among pixels of the whole image.

Brenner gradient function is the simplest gradient evaluation function, which simply calculates the square of the gray difference between two adjacent pixels.

$$D(f) = \sum_y \sum_x |f(x+2, y) - f(x, y)|^2 \tag{3}$$

where: $f(x, y)$ represents the gray value of pixel (x, y) corresponding to image f, and $D(f)$ is the result of image definition calculation (the same below).

SMD2 multiplies two gray variances in each pixel field and then accumulates them one by one.

$$D(f) = \sum_y \sum_x |f(x, y) - f(x+1, y)||f(x, y) - f(x, y+1)| \tag{4}$$

The Vollrath function is defined as follows

$$D(f) = \sum_y \sum_x |f(x, y) - \mu|^2 \tag{5}$$

Where: μ is the average gray value of the whole image, which is sensitive to noise. The purer the image, the smaller the function value.

The vollath function is defined as follows:

$$D(f) = \sum_y \sum_x f(x, y) \cdot f(x+1, y) - M \cdot N \cdot \mu^2 \tag{6}$$

where: μ is the average gray value of the whole image, M and N are the width and height of the image respectively.

Attribution analysis

The purpose of the integral gradient (IG) method is to quantify the contribution of each part of the input feature to the decision. For a given input image x and model $F(x)$, the goal of the network is to find out which pixels or features in x have an important influence on the decision-making of the model or sort the importance of each pixel or feature in x. Such a process is defined as attribution. IG uses the integral value along the whole gradient line from input to output. In the cell membrane segmentation task, for the decision of a pixel of y ((predicted as the cell membrane or not), we can get the contribution of each pixel of the input image $x_{i,j}$ to it. Put the contribution of each pixel together, we record it as an ***Attribution Field*** A, whose size is the same as the original image, and the value of each pixel is $w_{i,j}$ represents the contribution decision of pixel $x_{i,j}$ to y. $w_{i,j}$ is normalized to $[-1, 1]$.

In binary segmentation task, for the current input image x, if we know that the output y is a specific value, such as $y = 0$, and the corresponding reference image is x_i', then we can take a linear interpolation, that is

$$x' + \alpha \left(x - x'\right). \tag{7}$$

If the constant $\alpha = 0$, then the input image is the base image as x_i'. And if $\alpha = 1$, then the input image is the current image, which is x. When $0 \leq \alpha \leq 1$, it can be other images.

For the output of the neural network $F(x)$, the formula of the IG method is shown below.

$$A_i(F, x, x') = (x_i - x_i') \times \int_{\alpha=0}^{1} \frac{\delta F\left(x' + \alpha\left(x - x'\right)\right)}{\delta x_i} d\alpha \tag{8}$$

In formula 8, δx_i on the denominator denotes variation. This design makes the whole partial derivative transform into the form of variation. The variation boundary is the reference image and the current image, and the variation path can be selected arbitrarily. The integral gradient method uses linear interpolation as the variational path. That is,

$$\gamma(\alpha) = x' + \alpha \left(x - x'\right). \tag{9}$$

Here we select the random noise image as the reference image.

As the resolution and image size of U-RISC and ISBI 2012 is different, for a fair comparison, we also define the size of **Attribution Field** as S_k, which represents the real size of the actual biological neuron tissue corresponding to the pixel area with fixed contribution value threshold k. The pixels with higher contribution are divided by a selective threshold of k, that is, if the contribution value $w_{i,j}$ is greater than k, the pixel is the one with higher contribution to decision-making. Area of attribution field S_k is obtained by multiplying the area of attribution field value $w_{i,j} > k$ and the real tissue area (resolution h) corresponding to each pixel.

$$S_k = S(A_{w_{i,j}>k}) \times h^2, w_{i,j} \in A. \tag{10}$$

Data analysis

All statistical tests used, including statistic values and sample sizes, are provided in the figure captions, including mean and standard. All analyses were performed using custom software developed using the following tools and software: MATLAB (R2018a), Python (3.6), PyTorch (1.6.0), NumPy (1.19.0), SciPy (1.5.1), and matplotlib (2.2.3).

Acknowledgments

Additional information can be given in the template, such as to not include funder information in the acknowledgments section.

References

Adadi A, Berrada M. Peeking inside the black-box: a survey on explainable artificial intelligence (XAI). IEEE Access. 2018; 6:52138–52160.

Alejo R, Monroy de Jesús J, Pacheco Sánchez JH, López González E, Antonio Velázquez JA. A selective dynamic sampling back-propagation approach for handling the two-class imbalance problem. Applied Sciences. 2016; 6(7):200.

Amir A, McDonald D, Navas-Molina JA, Kopylova E, Morton JT, Xu ZZ, Kightley EP, Thompson LR, Hyde ER, Gonzalez A, et al. Deblur rapidly resolves single-nucleotide community sequence patterns. MSystems. 2017; 2(2).

Ancona M, Ceolini E, Öztireli C, Gross M. Gradient-based attribution methods. In: *Explainable AI: Interpreting, Explaining and Visualizing Deep Learning* Springer; 2019.p. 169–191.

Anderson JR, Jones BW, Yang JH, Shaw MV, Watt CB, Koshevoy P, Spaltenstein J, Jurrus E, Uv K, Whitaker RT. A Computational Framework for Ultrastructural Mapping of Neural Circuitry. Plos Biology. 2009; 7(3):e1000074.

Anderson JR, Jones BW, Watt CB, Shaw MV, Yang JH, DeMill D, Lauritzen JS, Lin Y, Rapp KD, Mastronarde D, et al. Exploring the retinal connectome. Molecular Vision. 2011; 17:355–79.

Arganda-Carreras I, Turaga SC, Berger DR, Cireşan D, Giusti A, Gambardella LM, Schmidhuber J, Laptev D, Dwivedi S, Buhmann JM, et al. Crowdsourcing the creation of image segmentation algorithms for connectomics. Frontiers in Neuroanatomy. 2015; 9:142.

Ashoor H, Chen X, Rosikiewicz W, Wang J, Li S. Graph embedding and unsupervised learning predict genomic sub-compartments from HiC chromatin interaction data. Nature Communications. 2020; 11(1).

Asuni N, Giachetti A. Accuracy improvements and artifacts removal in edge based image interpolation. VISAPP. 2008; 8:58–65.

Bach S, Binder A, Montavon G, Klauschen F, Müller KR, Samek W. On pixel-wise explanations for non-linear classifier decisions by layer-wise relevance propagation. PloS One. 2015; 10(7):e0130140.

Baehrens D, Schroeter T, Harmeling S, Kawanabe M, Hansen K, Müller KR. How to explain individual classification decisions. arXiv preprint arXiv:09121128. 2009; .

Barandela R, Valdovinos RM, Sánchez JS, Ferri FJ. The imbalanced training sample problem: Under or over sampling? In: *Joint IAPR International Workshops on Statistical Techniques in Pattern Recognition and Structural and Syntactic Pattern Recognition* Springer; 2004. p. 806–814.

Briggman KL, Bock DD. Volume electron microscopy for neuronal circuit reconstruction. Current Opinion in Neurobiology. 2012; 22(1):154–161.

Buades A, Coll B, Morel JM. A review of image denoising algorithms, with a new one. Multiscale Modeling and Simulation. 2005; 4(2):490–530.

y Cajal SR. Estructura de los centros nerviosos de las aves; 1888.

Castleman KR. Digital image processing. . 1993; .

Chaurasia A, Culurciello E. Linknet: Exploiting encoder representations for efficient semantic segmentation. In: *Proceedings of IEEE Visual Communications and Image*; 2017. p. 1–4.

Chen LC, Papandreou G, Kokkinos I, Murphy K, Yuille AL. Semantic image segmentation with deep convolutional nets and fully connected crfs. arXiv preprint arXiv:14127062. 2014; .

Chen W, Jiang Z, Wang Z, Cui K, Qian X. Collaborative global-local networks for memory-efficient segmentation of ultra-high resolution images. In: *Proceedings of the IEEE Conference on Computer Vision and Pattern Recognition*; 2019. p. 8924–8933.

Chen W, Jiang Z, Wang Z, Cui K, Qian X. Collaborative global-local networks for memory-efficient segmentation of ultra-high resolution images. In: *Proceedings of the IEEE Conference on Computer Vision and Pattern Recognition*; 2019. p. 8924–8933.

Choromanska A, Henaff M, Mathieu M, Arous GB, LeCun Y. The loss surfaces of multilayer networks. In: *Artificial Intelligence and Statistics*; 2015. p. 192–204.

Ciresan D, Giusti A, Gambardella LM, Schmidhuber J. Deep neural networks segment neuronal membranes in electron microscopy images. In: *Advances in Neural Information Processing Systems*; 2012. p. 2843–2851.

Ciresan D, Giusti A, Gambardella LM, Schmidhuber J. Deep neural networks segment neuronal membranes in electron microscopy images. In: *Advances in Neural Information Processing Systems*; 2012. p. 2843–2851.

Clark K, Khandelwal U, Levy O, Manning CD. What does bert look at? an analysis of bert's attention. arXiv preprint arXiv:190604341. 2019; .

Conrad R, Narayan K. CEM500K, a large-scale heterogeneous unlabeled cellular electron microscopy image dataset for deep learning. eLife Sciences. 2021; 10.

Cui Y, Jia M, Lin TY, Song Y, Belongie S. Class-balanced loss based on effective number of samples. In: *Proceedings of the IEEE Conference on Computer Vision and Pattern Recognition*; 2019. p. 9268–9277.

Curry A, Appleton H, Dowsett B. Application of transmission electron microscopy to the clinical study of viral and bacterial infections: present and future. Micron. 2006; 37(2):91–106.

Dando MR. Japan's Brain/MINDS project. In: *Neuroscience and the Problem of Dual Use*; 2020.p. 127–147.

Debello WM, Mcbride TJ, Nichols GS, Pannoni KE, Daniel S, Totten DJ. Input clustering and the microscale structure of local circuits. Frontiers in Neural Circuits. 2014; 8:112–.

DeFelipe, Javier. Neuroanatomy and Global Neuroscience. Neuron. 2017; 95(1):14–18.

Demir I, Koperski K, Lindenbaum D, Pang G, Huang J, Basu S, Hughes F, Tuia D, Raska R. Deepglobe 2018: A challenge to parse the earth through satellite images. In: *Proceedings of IEEE Conference on Computer Vision and Pattern Recognition Workshops*; 2018. p. 172–17209.

Dice LR. Measures of the amount of ecologic association between species. Ecology. 1945; 26(3):297–302.

Dong W, Zhang L, Lukac R, Shi G. Sparse representation based image interpolation with nonlocal autoregressive modeling. IEEE Transactions on Image Processing. 2013; 22(4):1382–1394.

Drozdzal M, Vorontsov E, Chartrand G, Kadoury S, Pal C. The importance of skip connections in biomedical image segmentation. In: *Deep Learning and Data Labeling for Medical Applications*; 2016.p. 179–187.

Erlandson RA. Role of electron microscopy in modern diagnostic surgical pathology. Modern Surgical Pathology. 2009; p. 71.

Feifei L, Fergus R, Perona P. One-shot learning of object categories. IEEE Trans Pattern Anal Mach Intell. 2006; 28(4):594–611.

Fernández A, Garcia S, Herrera F, Chawla NV. SMOTE for learning from imbalanced data: progress and challenges, marking the 15-year anniversary. Journal of Artificial Intelligence Research. 2018; 61:863–905.

Feyjie AR, Azad R, Pedersoli M, Kauffman C, Ayed IB, Dolz J. Semi-supervised few-shot learning for medical image segmentation. . 2020; .

Freixenet J, Muñoz X, Raba D, Martí J, Cufí X. Yet another survey on image segmentation: Region and boundary information integration. In: *European conference on computer vision*; 2002. p. 408–422.

Genovese CR, Perone-Pacifico M, Verdinelli I, Wasserman L, et al. Manifold estimation and singular deconvolution under Hausdorff loss. The Annals of Statistics. 2012; 40(2):941–963.

Gleeson A, Sawyer A, Mapping a brain; 2018.

Goceri E. Challenges and recent solutions for image segmentation in the era of deep learning. In: *International Conference on Image Processing Theory, Tools and Applications* IEEE; 2019. p. 1–6.

Golgi C. Sulla fina anatomia degli organi centrali del sistema nervoso. . 1885; .

Guidotti R, Monreale A, Ruggieri S, Turini F, Giannotti F, Pedreschi D. A survey of methods for explaining black box models. ACM computing surveys (CSUR). 2018; 51(5):1–42.

Halevy A, Norvig P, Pereira F. The unreasonable effectiveness of data. IEEE Intelligent Systems. 2009; 24(2):8–12.

Haralick RM, Shapiro LG. Image segmentation techniques. Computer vision, graphics, and image processing. 1985; 29(1):100–132.

Hariharan B, Arbeláez P, Girshick R, Malik J. Hypercolumns for object segmentation and fine-grained localization. In: *Proceedings of the IEEE Conference on Computer Vision and Pattern Recognition*; 2015. p. 447–456.

Harris KM, Perry E, Bourne J, Feinberg M, Ostroff L, Hurlburt J. Uniform serial sectioning for transmission electron microscopy. Journal of Neuroscience. 2006; 26(47):12101–12103.

Hashemi SR, Salehi SSM, Erdogmus D, Prabhu SP, Warfield SK, Gholipour A. Asymmetric loss functions and deep densely-connected networks for highly-imbalanced medical image segmentation: Application to multiple sclerosis lesion detection. IEEE Access. 2018; 7:1721–1735.

He F, Nie F, Wang R, Li X, Jia W. Fast Semisupervised Learning With Bipartite Graph for Large-Scale Data. IEEE Transactions on Neural Networks and Learning Systems. 2020; 31(2):626–638.

He H, Siu WC. Single image super-resolution using Gaussian process regression. In: *CVPR 2011*; 2011. p. 449–456.

He K, Fan H, Wu Y, Xie S, Girshick R. Momentum contrast for unsupervised visual representation learning. In: *Proceedings of the IEEE/CVF Conference on Computer Vision and Pattern Recognition*; 2020. p. 9729–9738.

He K, Zhang X, Ren S, Sun J. Deep residual learning for image recognition. In: *Proceedings of the IEEE Conference on Computer Vision and Pattern Recognition*; 2016. p. 770–778.

Helmstaedter M, Briggman KL, Denk W. High-accuracy neurite reconstruction for high-throughput neuroanatomy. Nature Neuroscience. 2011; 14(8):1081–1088.

Henry C, Azimi SM, Merkle N. Road segmentation in SAR satellite images with deep fully convolutional neural networks. IEEE Geoscience and Remote Sensing Letters. 2018; 15(12):1867–1871.

Hu J, Shen L, Sun G. Squeeze-and-excitation networks. In: *Proceedings of the IEEE Conference on Computer Vision and Pattern Recognition*; 2018. p. 7132–7141.

Hwang JW, Lee HS. Adaptive image interpolation based on local gradient features. IEEE Signal Processing Letters. 2004; 11(3):359–362.

Insel TR, Landis SC, Collins FS. The NIH brain initiative. Science. 2013; 340(6133):687–688.

J R, ANDERSON, S, MOHAMMED, B, GRIMM, B W, JONES, P, KOSHEVOY. The Viking viewer for connectomics: scalable multi-user annotation and summarization of large volume data sets. Journal of Microscopy. 2010; 241(1):13–28.

Jia D, Wei D, Socher R, Li LJ, Kai L, Li FF. ImageNet: A large-scale hierarchical image database. Proc of IEEE Computer Vision and Pattern Recognition. 2009; p. 248–255.

Kalchbrenner N, Blunsom P. Recurrent continuous translation models. In: *Proceedings of the 2013 conference on empirical methods in natural language processing*; 2013. p. 1700–1709.

Karimi D, Salcudean SE. Reducing the Hausdorff distance in medical image segmentation with convolutional neural networks. IEEE Transactions on Medical Imaging. 2019; 39(2):499–513.

Kaynig V, Vazquez-Reina A, Knowles-Barley S, Roberts M, Jones TR, Kasthuri N, Miller E, Lichtman J, Pfister H. Large-Scale Automatic Reconstruction of Neuronal Processes from Electron Microscopy Images. Medical Image Analysis. 2015; 22(1):77–88.

Kervadec H, Bouchtiba J, Desrosiers C, Granger E, Dolz J, Ayed IB. Boundary loss for highly unbalanced segmentation. In: *International conference on medical imaging with deep learning*; 2019. p. 285–296.

Kingma DP, Ba J. Adam: A method for stochastic optimization. arXiv preprint arXiv:14126980. 2014; .

Kokkinos I. Boundary detection using f-measure-, filter-and feature-(f 3) boost. In: *European Conference on Computer Vision*; 2010. p. 650–663.

Kornfeld J, Denk W. Progress and remaining challenges in high-throughput volume electron microscopy. Current Opinion in Neurobiology. 2018; 50:261–267.

Kosub S. A note on the triangle inequality for the Jaccard distance. Pattern Recognition Letters. 2019; 120:36–38.

Krizhevsky A, Sutskever I, Hinton GE. Imagenet classification with deep convolutional neural networks. Advances in Neural Information Processing Systems. 2012; 25:1097–1105.

Lee K, Zung J, Li P, Jain V, Seung HS. Superhuman accuracy on the SNEMI3D connectomics challenge. arXiv preprint arXiv:170600120. 2017; .

Leitch B. Ultrastructure of electrical synapses: review. Electron Microscopy Reviews. 1992; 5(2):311.

Li DC, Liu CW, Hu SC. A learning method for the class imbalance problem with medical data sets. Computers in Biology and Medicine. 2010; 40(5):509–518.

Lichtman JW, Pfister H, Shavit N. The big data challenges of connectomics. Nature Neuroscience. 2014; 17(11):1448–1454.

Lin P, Huang P, Huang P, Hsu H. Alveolar bone-loss area localization in periodontitis radiographs based on threshold segmentation with a hybrid feature fused of intensity and the H-value of fractional Brownian motion model. Computer Methods and Programs in Biomedicine. 2015; 121(3):117–126.

Lin TY, Goyal P, Girshick R, He K, Dollár P. Focal loss for dense object detection. In: *Proceedings of the IEEE International Conference on Computer Vision*; 2017. p. 2980–2988.

Lin W, Li Dong. Adaptive downsampling to improve image compression at low bit rates. IEEE Transactions on Image Processing. 2006; 15(9):2513–2521.

Lin Z, Wei D, Jang WD, Zhou S, Pfister H. Two Stream Active Query Suggestion for Active Learning in Connectomics. Springer, Cham. 2020; .

Liu K, Yeh C, Chung J, Chang C. A Motion Deblur Method Based on Multi-Scale High Frequency Residual Image Learning. IEEE Access. 2020; 8:66025–66036.

Liu L, Wu FX, Wang YP, Wang J. Multi-Receptive-Field CNN for Semantic Segmentation of Medical Images. IEEE Journal of Biomedical and Health Informatics. 2020; 24(11):3215–3225.

Liu S, Ding W, Liu C, Liu Y, Wang Y, Li H. ERN: edge loss reinforced semantic segmentation network for remote sensing images. Remote Sensing. 2018; 10(9):1339.

Liu Y, Chen K, Liu C, Qin Z, Luo Z, Wang J. Structured knowledge distillation for semantic segmentation. In: *Proceedings of the IEEE/CVF Conference on Computer Vision and Pattern Recognition*; 2019. p. 2604–2613.

Liu Y, Yu J, Han Y. Understanding the effective receptive field in semantic image segmentation. Multimedia Tools and Applications. 2018; 77(17):22159–22171.

Marin D, He Z, Vajda P, Chatterjee P, Tsai S, Yang F, Boykov Y. Efficient segmentation: Learning downsampling near semantic boundaries. In: *Proceedings of the IEEE/CVF International Conference on Computer Vision*; 2019. p. 2131–2141.

Mastronarde DN. Automated electron microscope tomography using robust prediction of specimen movements. Journal of Structural Biology. 2005; 152(1):36–51.

Mesner N, Ostir K. Investigating the impact of spatial and spectral resolution of satellite images on segmentation quality. Journal of Applied Remote Sensing. 2014; 8(1):083696.

Montavon G, Lapuschkin S, Binder A, Samek W, Müller KR. Explaining nonlinear classification decisions with deep taylor decomposition. Pattern Recognition. 2017; 65:211–222.

Morgan JL, Lichtman JW. Why not connectomics? Nature Methods. 2013; 10(6):494–500.

Niessen WJ, Bouma CJ, Vincken KL, Viergever MA. Error metrics for quantitative evaluation of medical image segmentation. In: *Performance Characterization in Computer Vision*; 2000.p. 275–284.

Okano H, Miyawaki A, Kasai K. Brain/MINDS: brain-mapping project in Japan. Philosophical Transactions of the Royal Society B Biological Sciences. 2015; 370(1668):20140310–20140310.

Peng H, Long F, Zhao T, Myers E. Proof-editing is the bottleneck of 3D neuron reconstruction: the problem and solutions. Neuroinformatics. 2011; 9(2):103–105.

Phillips PJ, Flynn PJ, Scruggs T, Bowyer KW, Worek W. Overview of the Face Recognition Grand Challenge. In: *IEEE Computer Society Conference on Computer Vision and Pattern Recognition*; 2005. .

Poo MM, Du JL, Ip N, Xiong ZQ, Xu B, Tan T. China Brain Project: Basic Neuroscience, Brain Diseases, and Brain-Inspired Computing. Neuron. 2016; 92(3):591–596.

Poo M, Du J, Ip NY, Xiong Z, Xu B, Tan T. China brain project: basic neuroscience, brain diseases, and brain-inspired computing. Neuron. 2016; 92(3):591–596.

Ribera J, Guera D, Chen Y, Delp EJ. Locating objects without bounding boxes. In: *Proceedings of the IEEE Conference on Computer Vision and Pattern Recognition*; 2019. p. 6479–6489.

Ronneberger O, Fischer P, Brox T. U-net: Convolutional networks for biomedical image segmentation. In: *International Conference on Medical Image Computing and Computer-Assisted Intervention*; 2015. p. 234–241.

Roy AG, Navab N, Wachinger C. Concurrent spatial and channel 'squeeze and excitation'in fully convolutional networks. In: *International Conference on Medical Image Computing and Computer-Assisted Intervention*; 2018. p. 421–429.

Russakovsky O, Deng J, Su H, Krause J, Satheesh S, Ma S, Huang Z, Karpathy A, Khosla A, Bernstein M. ImageNet Large Scale Visual Recognition Challenge. International Journal of Computer Vision. 2014; p. 1–42.

Sajjadi MS, Scholkopf B, Hirsch M. Enhancenet: Single image super-resolution through automated texture synthesis. In: *Proceedings of the IEEE International Conference on Computer Vision*; 2017. p. 4491–4500.

Salehi SSM, Erdogmus D, Gholipour A. Tversky loss function for image segmentation using 3D fully convolutional deep networks. In: *International workshop on machine learning in medical imaging*; 2017. p. 379–387.

Saltelli A, Annoni P, Azzini I, Campolongo F, Ratto M, Tarantola S. Variance based sensitivity analysis of model output. Design and estimator for the total sensitivity index. Computer Physics Communications. 2010; 181(2):259–270.

Schulz K, Sixt L, Tombari F, Landgraf T. Restricting the flow: Information bottlenecks for attribution. arXiv preprint arXiv:200100396. 2020; .

Shawn M. Progress Towards Mammalian Whole-Brain Cellular Connectomics. Frontiers in Neuroanatomy. 2016; 10.

Sheikh HR, Bovik AC, de Veciana G. An information fidelity criterion for image quality assessment using natural scene statistics. IEEE Transactions on Image Processing. 2005; 14(12):2117–2128.

Shorten C, Khoshgoftaar TM. A survey on image data augmentation for deep learning. Journal of Big Data. 2019; 6(1):1–48.

Shrikumar A, Greenside P, Kundaje A. Learning important features through propagating activation differences. In: *International Conference on Machine Learning*; 2017. p. 3145–3153.

Simonyan K, Zisserman A. Very Deep Convolutional Networks for Large-Scale Image Recognition. Computer Science. 2014; .

Simonyan K, Zisserman A. Very deep convolutional networks for large-scale image recognition. arXiv preprint arXiv:14091556. 2014; .

Smilkov D, Thorat N, Kim B, Viégas F, Wattenberg M. Smoothgrad: removing noise by adding noise. arXiv preprint arXiv:170603825. 2017; .

Sorensen, Thorvald. A method of establishing groups of equal amplitude in plant sociology based on similarity of species content and its application to analyses of the vegetation on Danish commons. Biol Skar. 1948; 5:1–34.

Spiring FA. The reflected normal loss function. Canadian Journal of Statistics. 1993; 21(3):321–330.

Srivastava N, Hinton G, Krizhevsky A, Sutskever I, Salakhutdinov R. Dropout: a simple way to prevent neural networks from overfitting. The Journal of Machine Learning Research. 2014; 15(1):1929–1958.

Stamatatos E. A survey of modern authorship attribution methods. Journal of the American Society for information Science and Technology. 2009; 60(3):538–556.

Subbarao M, Tyan J. Selecting the optimal focus measure for autofocusing and depth-from-focus. IEEE Transactions on Pattern Analysis and Machine Intelligence. 1998; 20(8):864–870. doi: 10.1109/34.709612.

Sudre CH, Li W, Vercauteren T, Ourselin S, Cardoso MJ. Generalised dice overlap as a deep learning loss function for highly unbalanced segmentations. In: *Deep Learning in Medical Image Analysis and Multimodal Learning for Clinical Decision Support*; 2017.p. 240–248.

Sundararajan M, Taly A, Yan Q. Axiomatic attribution for deep networks. In: *Proceedings of the 34th International Conference on Machine Learning*, vol. 70; 2017. p. 3319–3328.

Szegedy C, Liu W, Jia Y, Sermanet P, Reed S, Anguelov D, Erhan D, Vanhoucke V, Rabinovich A. Going deeper with convolutions. In: *Proceedings of the IEEE conference on computer vision and pattern recognition*; 2015. p. 1–9.

Takaya E, Takeichi Y, Ozaki M, Kurihara S. Sequential Semi-supervised Segmentation for Serial Electron Microscopy Image with Small Number of Labels. Journal of Neuroscience Methods. 2021; p. 109066.

Tan M, Le Q. Efficientnet: Rethinking model scaling for convolutional neural networks. In: *International Conference on Machine Learning*; 2019. p. 6105–6114.

Thakkinstian A, McElduff P, D'Este C, Duffy D, Attia J. A method for meta-analysis of molecular association studies. Statistics in Medicine. 2005; 24(9):1291–1306.

Urmson C, Whittaker W. Self-Driving Cars and the Urban Challenge. IEEE Intelligent Systems. 2008; 23(2):66–68.

Vaswani A, Shazeer N, Parmar N, Uszkoreit J, Jones L, Gomez AN, Kaiser L, Polosukhin I. Attention is all you need. . 2017; .

Veltkamp RC, Hagedoorn M. Shape similarity measures, properties and constructions. In: *International Conference on Advances in Visual Information Systems*; 2000. p. 467–476.

Vollath D. Nanomaterials an introduction to synthesis, properties and application. Environmental Engineering and Management Journal. 2008; 7(6):865–870.

Vu T, Van Nguyen C, Pham TX, Luu TM, Yoo CD. Fast and efficient image quality enhancement via desubpixel convolutional neural networks. In: *Proceedings of the European Conference on Computer Vision Workshops*; 2018. p. 0–0.

Wang R, Gong M, Tao D. Receptive field size versus model depth for single image super-resolution. IEEE Transactions on Image Processing. 2019; 29:1669–1682.

Wang Y, Chen Q, Zhang B. Image enhancement based on equal area dualistic sub-image histogram equalization method. IEEE Transactions on Consumer Electronics. 1999; 45(1):68–75.

Wang Z, Bovik AC. Modern image quality assessment. Synthesis Lectures on Image, Video, and Multimedia Processing. 2006; 2(1):1–156.

Wang Z, Simoncelli EP, Bovik AC. Multiscale structural similarity for image quality assessment. In: *The Thrity-Seventh Asilomar Conference on Signals, Systems and Computers, 2003*, vol. 2; 2003. p. 1398–1402.

White JG, Southgate E, Thomson JN, Brenner S. The structure of the nervous system of the nematode Caenorhabditis elegans. Philos Trans R Soc Lond B Biol Sci. 1986; 314(1165):1–340.

Wu X, Sahoo D, Hoi S. Recent Advances in Deep Learning for Object Detection. Neurocomputing. 2020; 396.

Wu X, Zhang X, Wang X. Low Bit-Rate Image Compression via Adaptive Down-Sampling and Constrained Least Squares Upconversion. IEEE Transactions on Image Processing. 2009; 18(3):552–561. doi: 10.1109/TIP.2008.2010638.

Yeghiazaryan V, Voiculescu ID. Family of boundary overlap metrics for the evaluation of medical image segmentation. Journal of Medical Imaging. 2018; 5(1):015006.

Yen SJ, Lee YS. Cluster-based under-sampling approaches for imbalanced data distributions. Expert Systems with Applications. 2009; 36(3):5718–5727.

Yoo J, Ahn N, Sohn KA. Rethinking data augmentation for image super-resolution: A comprehensive analysis and a new strategy. In: *Proceedings of the IEEE/CVF Conference on Computer Vision and Pattern Recognition*; 2020. p. 8375–8384.

Zhang K, Wu Z, Yuan D, Luan J, Jia J, Meng H, Song B. Re-weighted interval loss for handling data imbalance problem of end-to-end keyword spotting. Proceedings of Interspeech. 2020; p. 2567–2571.

Zhang YJ. A survey on evaluation methods for image segmentation. Pattern Recognition. 1996; 29(8):1335–1346.

Zhao H, Qi X, Shen X, Shi J, Jia J. Icnet for real-time semantic segmentation on high-resolution images. In: *Proceedings of the European Conference on Computer Vision*; 2018. p. 405–420.

Zhiding Yu, Chen Feng, Mingyu Liu, Ramalingam Srikumar. Casenet: Deep category-aware semantic edge detection. In: *Proceedings of the IEEE Conference on Computer Vision and Pattern Recognition*; 2017. p. 5964–5973.

Zhou Z, Siddiquee MMR, Tajbakhsh N, Liang J. Unet++: A nested u-net architecture for medical image segmentation. In: *Deep Learning in Medical Image Analysis and Multimodal Learning for Clinical Decision Support*; 2018.p. 3–11.

Zhu Z, Xu Z, You A, Bai X. Semantically multi-modal image synthesis. In: *Proceedings of the IEEE/CVF Conference on Computer Vision and Pattern Recognition*; 2020. p. 5467–5476.

Appendix 1

The Effects of Downsampling on U-RISC Dataset

To our best knowledge, downsampling is an effective approach to process images with enormous size in segmentation tasks (***Marin et al., 2019***; ***Chen et al., 2014***). With the purpose of investigating the effects of downsampling on image definition quality, we analyzed the gray-scale histograms on a group of original and downsampled images in U-RISC and then calculated the definition values of images in Track 2.

We first found that downsampling produced numerous mutations between adjacent gray values (***Figure 1***(C)). In our analysis, the mutations might engender the texture information in the image to be blurred, and the edges of the cell membrane became a blur. For example, the bilayer structure of the membrane disappeared after downsampled (***Figure 1*** (A,B)), and some of the cell membranes which were hard to recognizable became obscured. We then found that the defining quality of the images in Track 2 became lower after downsampled. Four definition indexes of all the images in Track 2 were calculated. Brenner (***Subbarao and Tyan, 1998***), Variance (***Subbarao and Tyan, 1998***), SMD2 (***Thakkinstian et al., 2005***), and Vollath (***Vollath, 2008***) are common indexes to show the gray value change between adjacent pixels. Results suggested that image indexes were significantly decreased after downsampling (***Figure 1***(D)), and all the four indexes dropped about ten times. Therefore, the analysis indicated that images were heavily blurred after the downsampling operation.

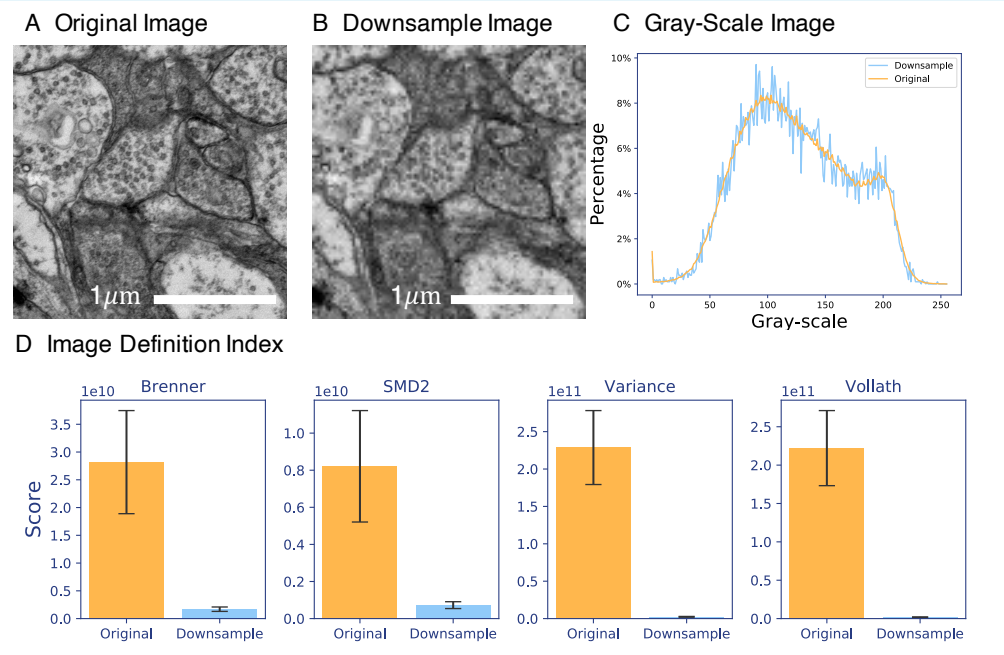

Appendix 1 Figure 1. Differences between original image and downsampled image.(A) The crop of original image. (B) The crop of downsampled image at the same position. The Gray-scale Histograms is calculated on A and B. (C) The scores of definition indexes calculated on the whole U-RISC dataset before and after downsampling. Details of indexes are described in Methods and Materials.

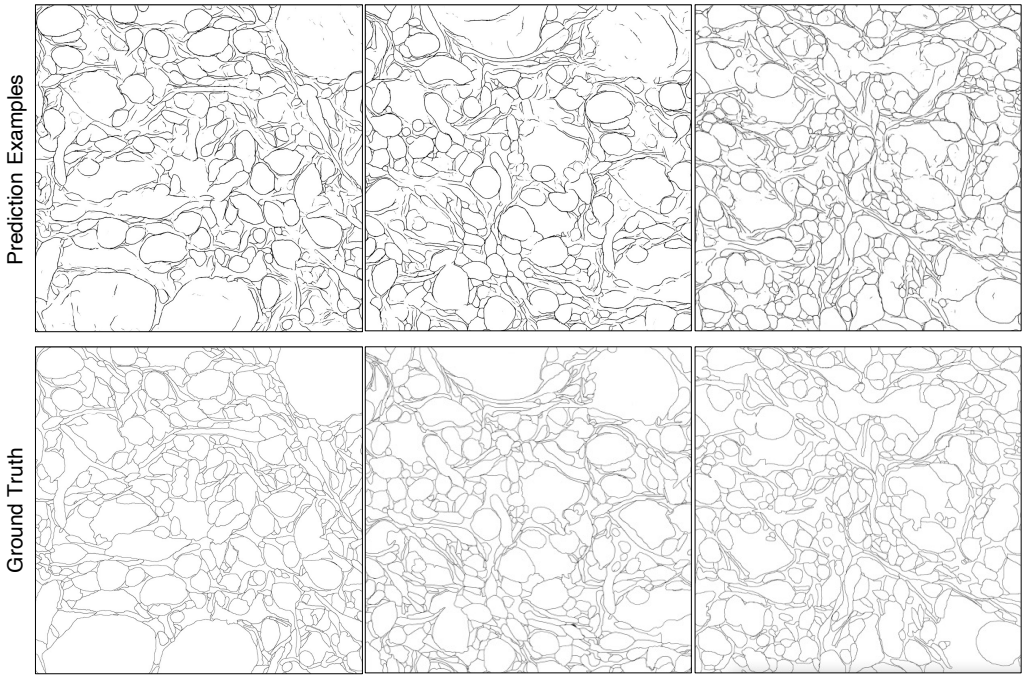

Figure 6–Figure supplement 1. Supplements for segmentation predictions of U-RISC.

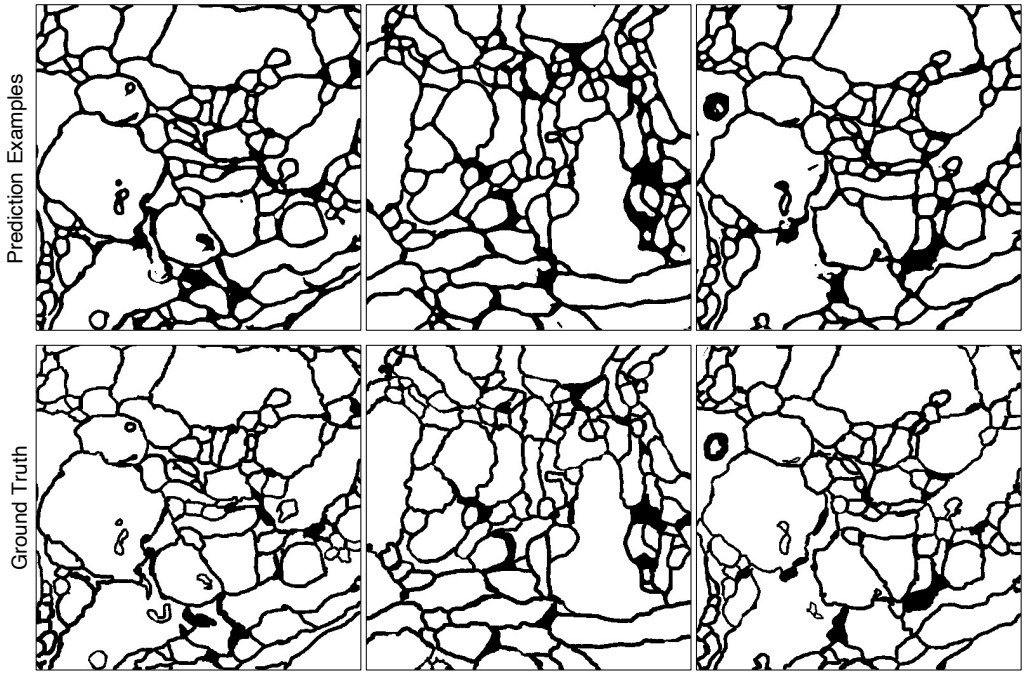

Figure 6–Figure supplement 2. Supplements for segmentation predictions of ISBI 2012.

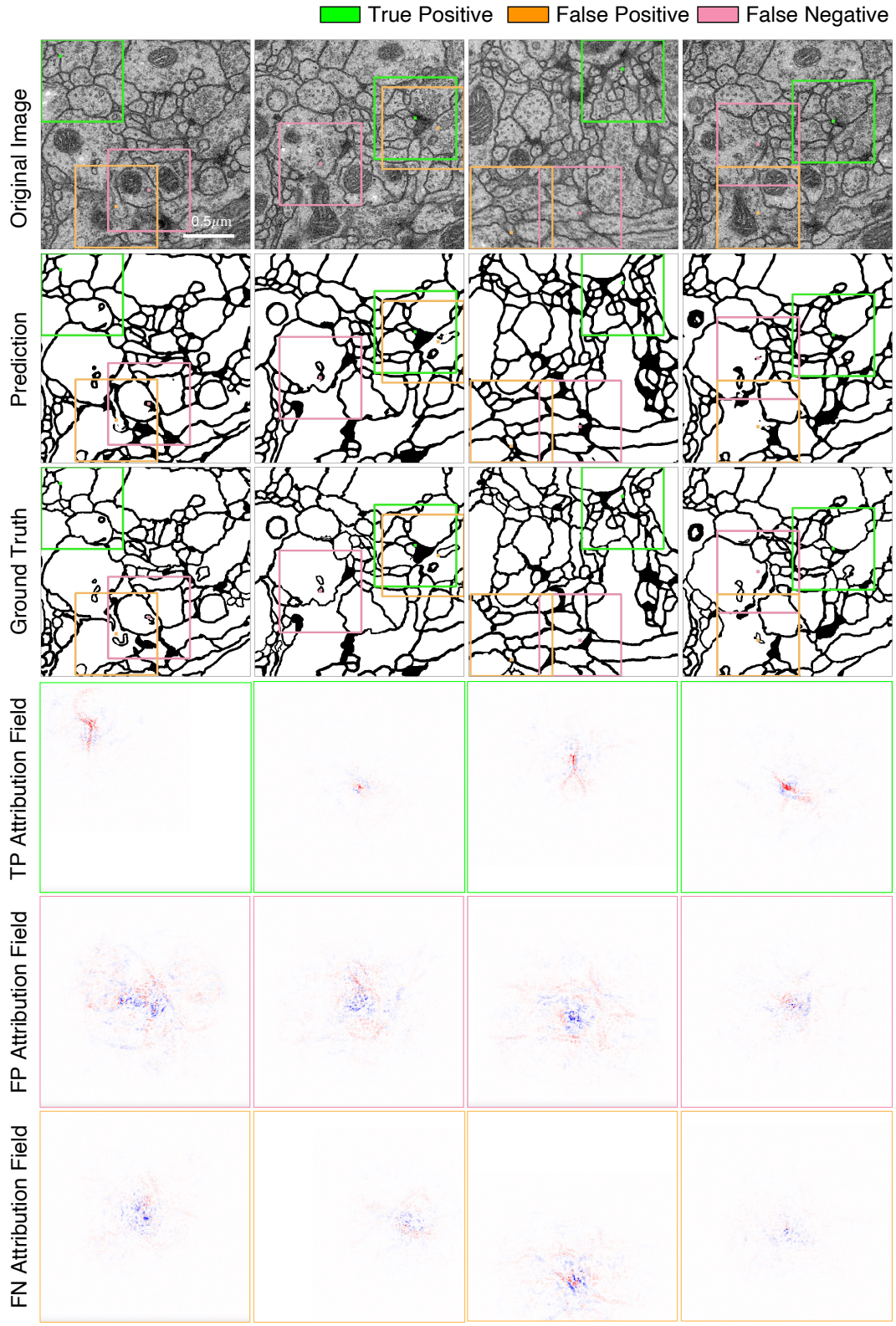

Figure 8–Figure supplement 1. Supplements for attribution analysis on ISBI 2012.

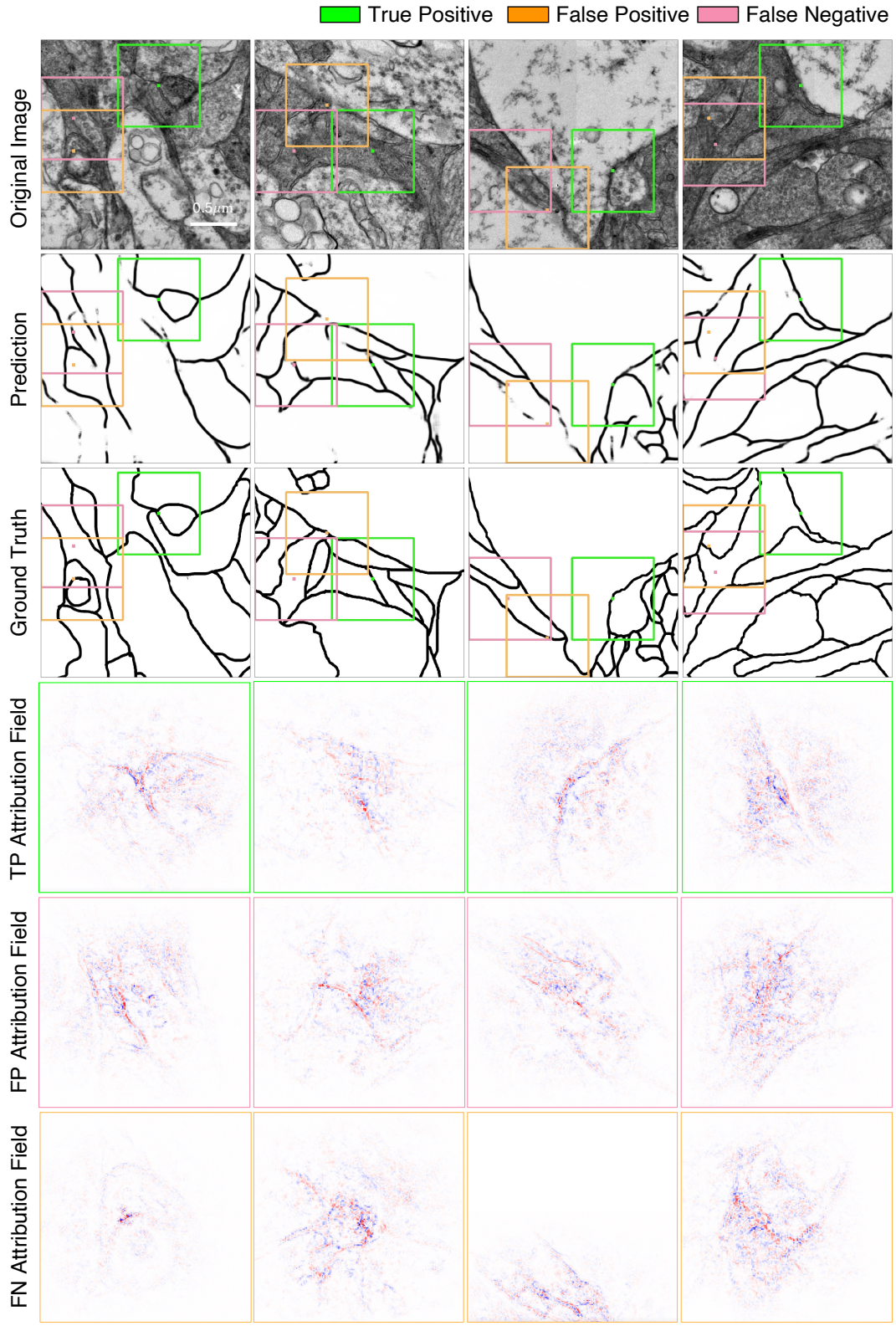

Figure 8–Figure supplement 2. Supplements for attribution analysis on U-RISC.